Korean J. Chem. Eng., **29**(2), 249-262 (2012)
DOI: 10.1007/s11814-011-0158-6

Adsorptive separation of carbon dioxide by polyethyleneimine modified adsorbents

Pankaj Sharma*, Il-Hyun Baek*†, Ye-Won Park*, Sung-Chan Nam*, Jeong-Hun Park*, Sang-Do Park, and Sung Youl Park***

*Greenhouse Gas Research Center, **Carbon Dioxide Reduction & Sequestration R&D Center,
Korea Institute of Energy Research, 71-2, Jang-dong, Yuseong-gu, Daejeon 305-343, Korea
(*Received 11 December 2010 • accepted 10 June 2011*)

Abstract−Utilization of carbon dioxide (CO_2) has become an important global issue due to significant and continuous rise in atmospheric CO_2 concentrations. To find a potential solution, two types of mesoporous materials, MCM-41 and MCM-48, were synthesized and impregnated with 30, 50 and 70 wt% of polyethyleneimine (PEI) in methanol to evaluate the performance of the materials in terms of CO_2 adsorption. The materials were characterized by XRD, TGA, FT-IR, TEM, SEM, N_2-physisorption and BET techniques. All the PEI-loaded materials exhibited substantially higher reversible CO_2 adsorption-desorption behaviors with >99% recovery. The above study proved that MCM-48 is a better material as compared to MCM-41 for loading of PEI. The material with 50 wt% loading of PEI on MCM-48, showed maximum adsorption of 248 mg/g-PEI at 80 °C which is about 30 times higher than that of MCM-48 and about 2.3 times that of pure PEI.

Key words: Carbon Dioxide Removal, PEI (Polyethyleneimine), MEA (Monoethanolamine), Mesoporous Material, MCM-41, MCM-48

INTRODUCTION

The term "greenhouse" has been mentioned quite often in the recent literature, as a result of society's concern over rising atmospheric temperature. While there are several compounds which contribute to the greenhouse effect, carbon dioxide (CO_2) has received the most attention, due to its abundance as part of the effluent from many industrial processes. The emission of CO_2 is one of the serious environmental problems due to its significantly increased concentration in the past five decades and most notably in last 15 years [1]. CO_2 has been identified as a greenhouse gas that contributes to global climate change and global warming. According to the third assessment report of the Intergovernmental Panel on Climate Change (IPCC), there has been a global increment of the atmospheric concentration of CO_2 by about 100 ppm (36%) over the last 250 years, from a range of 275-285 ppm in the pre-industrial era (1,000-1,750) to 379 ppm in 2005 [2]. The highest average growth rate of atmospheric CO_2 concentration was recorded from 1995 to 2005 (19 ppm increment) for any decade since direct atmospheric CO_2 measurement began in the 1950s [3]. The main source of emission of CO_2 is burning of fuel, such as natural gas, coal and petroleum for the production of electricity and transportation [4]. The emission of CO_2 can be reduced through several ways such as replacement of fossil fuel with environmental friendly biofuel, improvement in energy efficiency and sequestration of CO_2 from its source [5]. CO_2 removal from the natural gas stream and flue gas discharged by the power plants has received considerable attention in recent years [6].

The conventional technologies for removal of CO_2 are cryogenic distillation, amine absorption [7-9] and absorbent liquid absorption through membrane contactor [10]. Amine absorption is a widely developed commercial technology for CO_2 removal. However, there are a number of drawbacks to using amine type liquid absorbent, such as high energy consumption for solvent regeneration, equipment corrosion and flow problems caused by viscosity [11,12]. After removal of CO_2 from its source such as flue gas via capture by amine absorption, an additional step is needed to isolate and regenerate the solvent. Owing to the high cost of regeneration process [13], regenerable solid adsorbents appear to be alternative for CO_2 adsorption over the conventional methods. Physical adsorbents based on carbons and zeolites are able to reversibly adsorb large quantity of CO_2 at room temperature [11]. However, these physical adsorbents have several disadvantages such as reduced CO_2 adsorption capacity at high temperature [11,12], requirement of high temperature regeneration and poor tolerance to water [14].

Recently, there has been increased interest in developing mesoporous materials (molecular sieve) for adsorption of CO_2 due to their high porosity to facilitate rapid gas diffusion to and from their surface [15]. Their pores are large enough to be accessible for various functional groups. The introduction of functional groups such as amine groups to these mesoporous materials to create specific interactions with CO_2 has gained importance to overcome the disadvantages of the conventional amine absorption processes [16]. Mesoporous materials offer scope for surface modification aimed at enhancing CO_2 adsorption compared to microporous materials such as zeolites. The microporous materials with small pores might not allow the access of functional groups or even forbid the passage of large target gas molecules [17,18].

In addition, various amine functional groups have been studied for functionalization of the ordered mesoporous silica materials to enhance CO_2 adsorption, in view of the high affinity and interaction between the amine groups and CO_2 [19,20].

On the other hand, recent discovery of a new family of mesoporous molecular sieves named M41S has been receiving much attention

†To whom correspondence should be addressed.
E-mail: ihbaek@kier.re.kr

after it was introduced by Mobil researchers [21]. The M41S family is classified into several members: MCM-41, MCM-48, MCM-50 and other species. MCM-41 has a hexagonal array of unidirectional pores. while MCM-48 has a bicontinuous cubic pore system [22]. Their synthesis and utilization have been investigated by many researchers because of their peculiar characteristics such as large internal surface area, uniformity of pore size, easily controlled size of pores, tunable surface chemistry via functionalization and high thermal stability. These mesoporous materials are useful as adsorbents [23,24], and supports [25]. Moreover, the interwoven and branched pore structure of MCM-48 provides more favorable mass transfer kinetics than MCM-41 [26]. Therefore, MCM-48 seems to be a better candidate as an adsorbent in separation techniques or as a catalyst support than MCM-41. In the past few years, many investigations have been conducted on the synthesis [26,27], characterization [22], mechanical stability [23,28] and adsorption characteristics of MCM-41 and MCM-48. Surface functionalization of mesoporous materials with several types of functional groups for application in adsorption and catalysis has been recently reported [29-31]. The introduction of basic sites into the pore channels of mesoporous silica to enhance CO_2 adsorption has been recently investigated by several groups. Shen et al. studied CO_2 adsorption over MCM-41 modified with La_2O_3 [32]. Huang et al. reported acid gas removal from natural gas using aminopropylattached MCM-48 [33]. Chaffee et al. attached various amines to the pores of hexagonal mesoporous silicas (HMS) and characterized them with respect to CO_2 adsorption in a short communication [34]. However, the attachment of various types of amino groups to the surface of mesoporous materials and their CO_2 adsorption properties have not yet been systematically investigated in these brief communications [32-34].

Recently, a new concept of CO_2 "molecular basket" has been proposed by C. Song and coworkers for developing high-capacity, highly-selective CO_2 adsorbents [35-37]. The CO_2 molecular basket adsorbents can selectively "pack" CO_2 in condensed form in the mesoporous molecular sieve basketand therefore shows a high CO_2 adsorption capacity and a high CO_2 selectivity. In their work, the sterically branched polymer of polyethylenimine (PEI), which has branched chains with numerous CO_2-capturing sites such as amine groups, was loaded into the large pore volume porous material of mesoporous molecular sieve MCM-41 type to make the molecular basket adsorbent.

The present work included the synthesis of mesoporous materials, MCM-41 and MCM-48, loaded with 30, 50 and 70 wt% of PEI to synthesize the novel molecular basket adsorbent. The textural and physico-chemical properties of scaffold and impregnated materials were characterized by X-ray diffraction (XRD), thermogravimetric analysis (TGA), Fourier transform-infra red (FT-IR), transmission electron microscopy (TEM), scanning electron microscopy (SEM), N_2-physisorption and Brunner-Emmet-Teller (BET) techniques. In this report, we investigate the pore structures and CO_2 adsorption properties of several MCM-41 and MCM-48 adsorbents, functionalized with different wt% loading of PEI. The CO_2 adsorption/desorption performance of the materials synthesized by loading different wt% of PEI has been evaluated by TGA. Among two adsorbents, MCM-41 and MCM-48, the best one for loading of PEI is proposed. The wt% loading of PEI for maximum CO_2 capture as well as selectivity have been optimized. This report also includes a comparison of the adsorption capacity of PEI loded on MCM-41/48 materials with monoethanolamine (MEA). The physico-chemical properties of PEI and MEA are enlisted in Table 1. The fundamental insights obtained in this study are expected to assist in the rational design of novel functionalized M41S adsorbent materials for CO_2 separation from dilute sources.

Table 1. Physical properties of MEA and PEI

Property	MEA	PEI
Mol. weight	61.4	600
Density (g/ml)		1.03
Boiling point (°C)	171	250
Vapor pressure (mmHg) at 20 °C	0.36	9
Structure	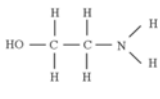	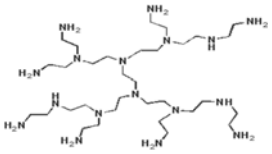

EXPERIMENTAL

1. Materials

2. Synthesis of MCM-41

MCM-41 was synthesized using CTABr, a cationic surfactant, and Ludox-40, a colloid silica, as the silica source. Distilled water was poured into two sample Teflon bottles. Ludox-40 and NaOH were added to sample bottle 1 labeled as solution A and NH_4OH was added to CTABr in sample bottle 2 labeled as solution B. Both bottles were agitated at 80 °C for 30 min; then the contents of both sample bottles were mixed, and the mixed solution was titrated to pH 11 using 1 M HCl or NaOH to promote hydrothermal synthesis. The synthesized material was filtered, washed with ionic water, and dried overnight at 60 °C. The dried sample was calcinated at 550 °C at a rate of 10 °C/min, for 6 h. The material thus finally obtained was labeled as MCM-41.

3. Synthesis of MCM-48

MCM-48 was synthesized, as with MCM-41, using CTABr and Ludox-40. Distilled water was poured into two sample Teflon bottles. Ludox-40 and NaOH were added to sample bottle 1 labelled as solution A and the bottle was agitated at 60 °C for 1 h. LE-4 was added to CTABr in sample bottle 2 labelled as solution B and the bottle was agitated at 40 °C for 20 min; then the contents of both sample bottles were mixed to promote hydrothermal synthesis at 100 °C for 78 h. The white precipitates created after hydrothermal synthesis were recycled through suction filtering washed with ionic water, and dried overnight at 60 °C. The dried sample was calcinated at 600 °C at a rate of 10 °C/min, for 10 h. The material thus finally obtained was labeled as MCM-48.

4. Synthesis of PEI Impregnated MCM-41 Materials

A series of mesoporous materials containing 30, 50 and 70 wt% PEI were synthesized by impregnation. 1 g of MCM-41 was taken and using a vacuum evaporator, a 30 wt% solution of PEI (0.3 g/10 ml of methanol) was gradually added and agitated. Finally, the slurry-like material was left over at 25 °C for 24 h. later. It was dried

in a vacuum oven at 75 °C for 16 h. The obtained material was designated as 30 wt%PEI-MCM-41-PEI. Similarly, mesoporous materials containing 50 and 70%wt PEI were obtained and designated as 50 wt%PEI-MCM-41-PEI and 70 wt%PEI-MCM-41-PEI, respectively.

5. Synthesis of PEI Impregnated MCM-48 Materials

A series of mesoporous materials containing 30, 50 and 70 wt% PEI were synthesized by impregnation. 1 g of MCM-48 was taken and using a vacuum evaporator, a 30 wt% solution of PEI (0.3 g/10 ml of methanol) was gradually added and agitated. Finally, the slurry-like material was left over at 25 °C for 24 h. later, It was dried in a vacuum oven at 75 °C for 16 h. The obtained material was designated as 30 wt%PEI-MCM-48-PEI. Similarly, mesoporous materials containing 50 and 70 wt% PEI were obtained and designated as 50 wt%PEI-MCM-48-PEI and 70 wt%PEI-MCM-48-PEI, respectively.

6. Characterization

The EDX analysis was done using Oxford INCA 250 energy dispersive X-ray microanalyzer.

Powder X-ray diffraction patterns (XRD) were recorded using a Rigaku Miniflex diffractometer (Model:M/N: D/Max lllC) with Cu Kα radiation (λ=0.154 nm). The diffraction data were recorded in the 2θ range of 0.5-10° at 0.02° step size and 1 s step time.

The thermal stability of the materials was analyzed by thermogravimetric analysis (TGA) on a TA Instrument Co. (Model: M/N: SDT Q600). The materials were poured onto a sample pan and then nitrogen gas flowed at 100 ml/min for one hour to remove the impurities and later materials were heated from 25 to 900 °C in steps of 1°/min in N_2 atmosphere at a flow rate of 20 ml/min.

Fourier transform infrared spectroscopy (FT-IR) of the samples was recorded at room temperature on a Thermo electron Co. spectrometer: (Model: M/N: NICOLET 6700). For the analysis, the background in the air was measured; then the adsorbent was added to the KBr and scanned 32 times over a frequency range of 400-4,000 cm^{-1}.

The surface morphology of the synthesized materials was studied by scanning electron microscopy (SEM) after gold coating on an instrument by Hitachi Co. (Model: M/N: S-4700). The voltage was 20 keV, and the field electron source was scanned at a resolution of 2 nm. Transmission electron microscopy (TEM) (Model: JEOL, JEM-2010) was used to study the morphology of the pure and modified materials.

The nitrogen adsorption-desorption isotherms were measured at −196 °C on a Micromeritics Co. (Model: M/N: ASAP 2010) volumetric adsorption analyzer. To remove the impurities, the sample was preprocessed at 150 °C for 2 h under vacuum ($p<10^{-5}$ mbar) in the degas port. After preprocessing, adsorption and desorption were performed using N_2. The specific surface area, S_{BET}, was determined from the linear part of the Brunauer-Emmett-Teller (BET) equation and the calculation of pore size distribution was performed using Barret-Joyner-Halenda (BJH) equation [9,10].

7. CO_2 Adsorption

The CO_2 adsorption/desorption performance of the materials was performed on a thermal gravimetric analysis (TGA), TA Instrument Co. (Model: M/N: SDT Q600). A sample weight of ca. 10 mg was loaded into an alumina sample pan in a TG unit and tested for CO_2 adsorption-desorption performance. The initial activation of the samples was carried out at 105 °C for 1 h in N_2 atmosphere at a rate of 100 ml/min. Then adsorption run was carried out using high purity CO_2 (99.999%) gas, while the desorption run was conducted in N_2 flow. Both the gases, CO_2 and N_2, were passed through an automatic valve, assisted with timer for continuous adsorption and desorption profile. The test was repeated 20 times after an adsorbent in the optimum condition had been selected.

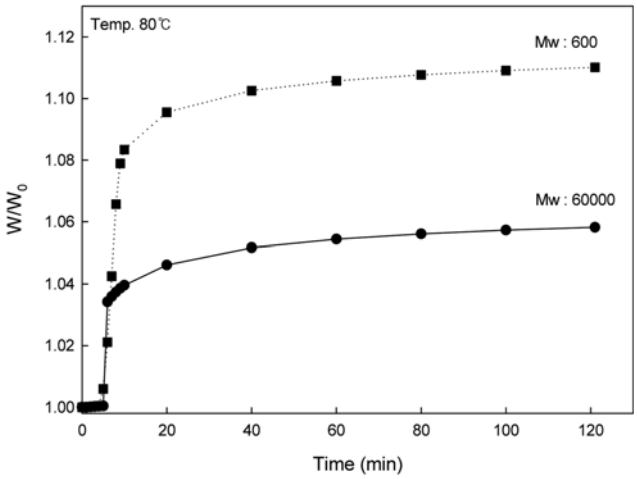

Fig. 1. Comparison of the CO_2 capacity according to PEI molecular weight.

RESULTS

1. Effect of PEI Molecular Weight

To improve the surface of the mesoporous adsorbent, PEI was selected as the material for impregnation. First, the CO_2 adsorption capability per PEI molecular weight was studied. The average molecular weight of the PEI was 60,000 and 600. To study the performance, adsorption at 80 °C was tested using a 50wt%-impregnated mesoporous adsorbent. Fig. 1 shows the results of the test. When the molecular weight of the PEI was 600 and 60.000, adsorption over two hours was 58.2 and 110.1 mg/g, respectively. This indicates that the adsorption of PEI with a smaller molecular weight was twice that of PEI with a heavier molecular weight. Such a phenomenon corresponds to the decrease in the solubility of the polymers as the molecular weight increases. When amines with a smaller molecular weight are impregnated, they are more uniformly distributed on the adsorbent surface, and have a higher adsorption capacity than those with a higher molecular weight.

2. Characterization

The powder XRD patterns of MCM-41, MCM-48 and PEI impregnated materials are presented in Fig. 2(a)-(b). The typical XRD patterns of MCM-41 (Fig. 2(a)) displayed Bragg peaks corresponding to hexagonal mesophase in the 2θ below 5°, which can be indexed to (100), (110), (200) and (210), the reflections and peaks beyond 5° are weak or absent due to local disorder. These d-spacings values indicate that MCM-41 structure possesses the hexagonal p6m space group. The typical XRD patterns of MCM-48 (Fig. 2(b)) displayed Bragg peaks corresponding to cubic mesophase in the 2θ between 1.5-8°, which can be indexed to different hkl reflections. These d-spacings values indicate that MCM-48 structure possesses the

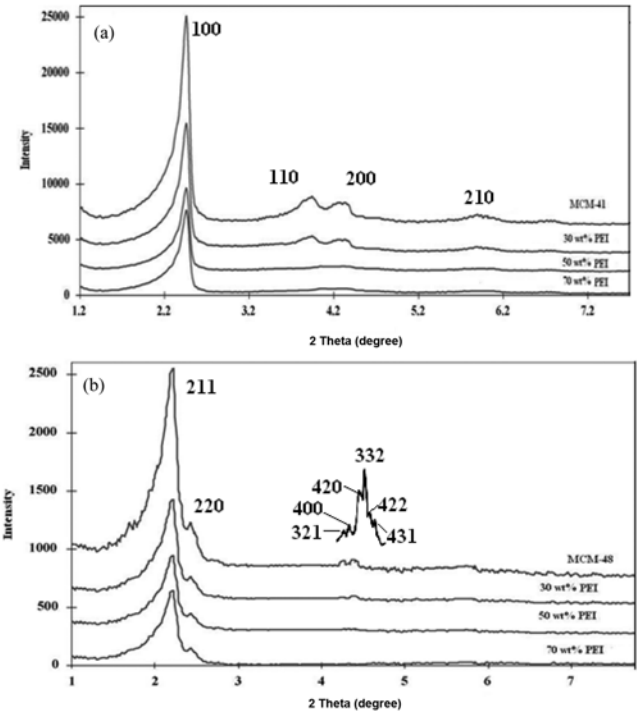

Fig. 2. XRD patterns of PEI impregnated mesoporous and impregnated materials: (a) MCM-41, (b) MCM-48.

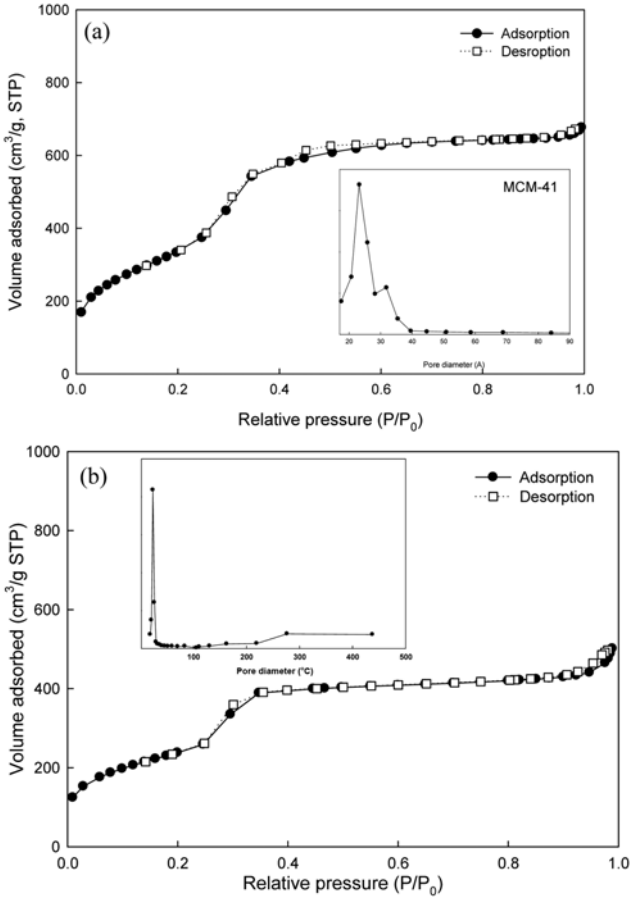

Fig. 3. N_2 adsorption-desorption isotherms of (a) MCM-41 and (b) MCM-48.

cubic Ia3d space group. The XRD patterns of the MCM-48 materials consisted of the typical reflection at 2.5° (211) and weak reflections at 2.9° (220), 4.7° (420), and 4.9° (332) which corresponded to the d-spacings of ca.34.8, 30.3, 18.8 and 19.0 Å, respectively. For the cubic structure of MCM-48, the highly ordered array of the solid could be inferred from the presence of a well defined set of diffraction peaks between 4° and 6° in the XRD pattern (321), (400), (420), (322), (422) and (431). The diffraction patterns of MCM-41 and MCM-48 didn't change significantly after PEI was impregnated, also confirming that the structure of the MCM-41 and MCM-48 mesoporous materials is stable. The position of the characteristic Bragg diffraction peak of each material remains nearly constant, indicating that the mesoporous structures of materials are preserved after impregnation of PEI. The peak intensity of MCM-41 and MCM-48, however, decreased slightly after impregnation of PEI. The peaks with higher hkl indices, i.e., (420) and (332), almost disappeared completely, whereas the peaks of MCM-41 and MCM-48 at (210), (211) and (220) shifted to a slightly lower 2θ angle. Generally, in case of M41S materials, the peak intensity is a function of the scattering contrast between the silica walls and pore channels, and it decreases with decreasing scattering contrast after impregnation of organic groups to the pore surface. Therefore, the observed decrease in intensity is probably due to pore filling by PEI, indicating that PEI was loaded into the channels of MCM-41 and MCM-48. Disappearance of higher hkl peaks may be due to lower structural order of PEI impregnated materials.

The N_2 adsorption-desorption isotherms of MCM-41 and MCM-48 are represented in Fig. 3(a)-(b) and isotherms of PEI impregnated MCM-41 and MCM-48 materials are reported in Fig. 4(a)-(b). The N_2 adsorption-desorption of MCM-41 (Fig. 3(a)) shows IUPAC Type IV isotherm with a sharp step up in a narrow range of relative pressure (P/P_o=0.2-0.4) arising from the capillary condensation of N_2 in channels of MCM-41 (hexagonal) structure. Similar to MCM-41, the N_2 adsorption-desorption of MCM-48 shows IUPAC Type IV isotherm (Fig. 3(b)) with a sharp step up in a narrow range of relative pressure, P/P_0=0.2-0.4, indicating capillary condensation of nitrogen in channels of MCM-48 (cubic) structure. The sharpness of the capillary condensation steps in MCM-41 and MCM-48 indicates the uniformity of pore channels and their narrow size distribution. The isotherm is reversible and doesn't exhibit hysteresis between adsorption and desorption. Also, the pore size distribution of MCM-41 and MCM-48 materials obtained from their desorption isotherms using the BJH method, is shown in Fig. 3(a)-(b). The determined average pore diameters of MCM-41 and MCM-48 according to BJH method were around 27 and 30 Å, respectively. And according to XRD d spacing, the values were 37.7 and 41.2 Å, respectively. The isotherms of PEI impregnated on MCM-41 (Fig. 4(a)) and MCM-48 (Fig. 4(b)) show IUPAC Type I adsorption isotherm, which is characteristic of microporous materials. The study of isotherms reveals that the mesoporous character of the MCM-41 and MCM-48 reflected in an S-shaped adsorption isotherm was lost after the impregnation of PEI on the surface of materials. The 30-50-70 wt% concentration of PEI on MCM-41 and MCM-48 showed the presence of microporosity, which demonstrates the effect of the PEI on the pore structure of MCM-41 and MCM-48. A significant

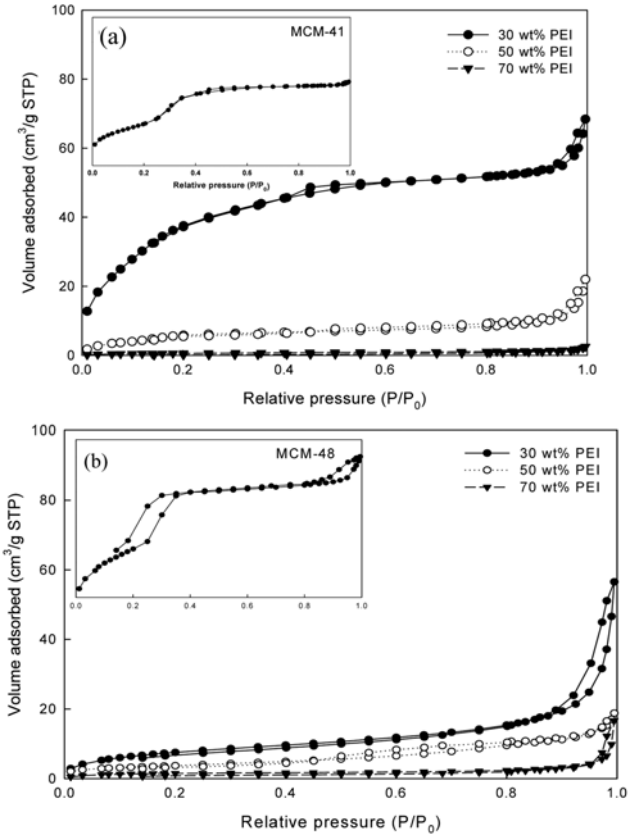

Fig. 4. N_2 adsorption-desorption isotherms of mesoporous and impregnated materials: (a) MCM-41, (b) MCM-48.

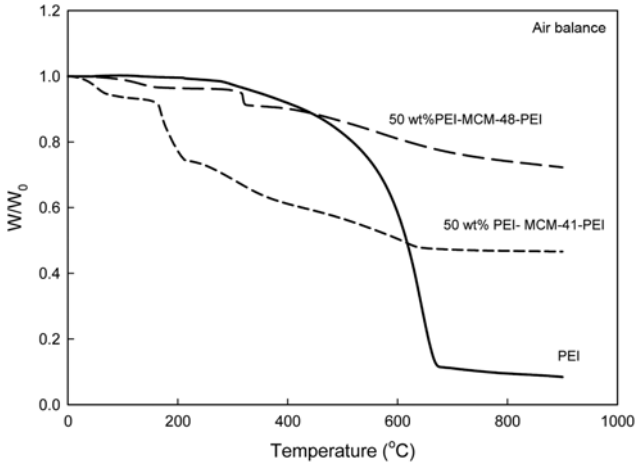

Fig. 5. TGA of pure PEI and MCM-41, MCM-48 impregnated materials.

decrease in the surface areas and pore volumes was also observed upon PEI impregnation. The specific BET surface area, pore volumes and pore sizes of MCM-41, MCM-48 and impregnated materials are summarized in Table 2. As compared to 30 wt% PEI loading, the 50 wt% PEI loading showed a more significant decrease of surface area and pore volume, probably due to significant pore filling with PEI. In particular, 70 wt% PEI loading material lost nearly all surface area and pore volume after impregnation, which indicated nearly complete pore filling, thus restricting access of nitrogen into the pores at the liquid nitrogen temperature. Therefore, information on the meaningful textural properties cannot be obtained from N_2 adsorption-desorption isotherms for PEI loading higher than the maximum of 50 wt% PEI loading. So, samples having 50 wt% concentration of PEI were selected for further study and characterization. The values of surface area, pore volume and average pore diameter (Table 2) of MCM-48 are greater than MCM-41, and all these combined features enable MCM-48 to better accommodate the bulky PEI with little hindrance and allow higher loading inside channels as compared to MCM-41.

Fig. 5 shows TGA of pure PEI and 50 wt% PEI loaded on MCM-41 and MCM-48. The pure PEI loses ca. 2 wt% weight near 100 °C due to desorption of CO_2 and moisture and a sharp weight loss of 90% appeared from 300 to 680 °C, which indicates complete decomposition of PEI at 680 °C. PEI loaded on MCM-41 and MCM-48 samples showed weight loss below 100 °C associated with physically adsorbed water. Above 100 °C, they showed additional weight loss associated with condensation of surface silanol groups between 150-325 °C. This weight loss is more intense in MCM-41 samples as compared to MCM-48 samples. Above this temperature, they exhibited a weight loss behavior very different from that of the pure PEI sample. The weight loss above 325 °C was associated with the

Table 2. Surface area, pore diameter and pore volume of mesoporous materials with PEI impregnation amount

Materials	PEI amount (wt%)	Surface area (m^2/g)	Pore diameter (Å)	Pore volume (m^3/g)	Amine efficiency
MCM-41	-	1419	27.1[a]	1.155	
			37.7[b]		
MCM-41-PEI	30	149	23.9	0.106	0.6
	50	116	27.1	0.034	1.2
	70	2.27	47.2	0.004	0.9
MCM-48	-	829	30.4[a]	1.230	
			41.2[b]		
MCM-48-PEI	30	29.1	67.2	0.048	1.2
	50	5.58	61.8	0.025	2.2
	70	2.31	67.9	0.029	1.9

[a]Obtained from BJH method
[b]Obtained from XRD d spacing

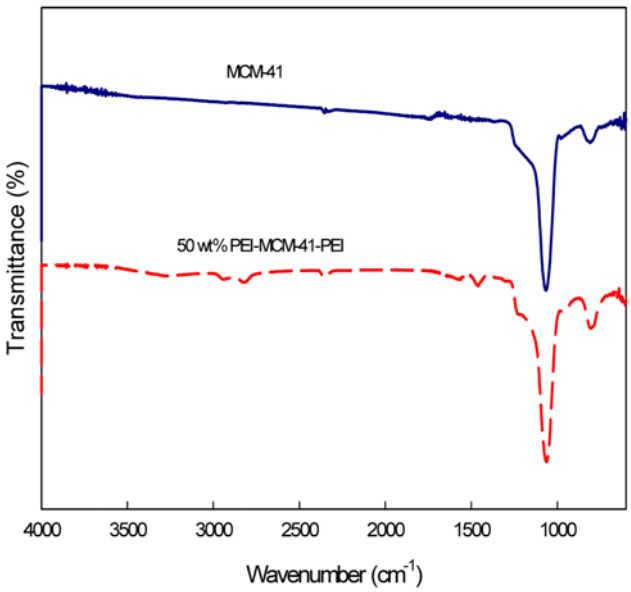

Fig. 6. FT-IR of MCM-41 and 50 wt% PEI-MCM-41-PEI.

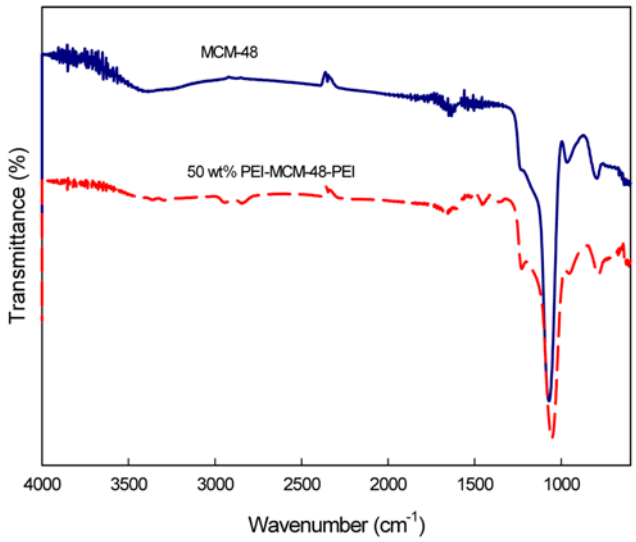

Fig. 7. FT-IR of MCM-48 and 50 wt% PEI-MCM-48-PEI.

decomposition of the surface attached PEI as well as the condensation of SiOH groups. TGA studies also show that MCM-48 is a better support than MCM-41. These results are in good agreement with the pore volume and average pore diameter analysis data.

The FT-IR spectra of pure MCM-41, MCM-48 and PEI loaded samples are reported in Fig. 6. The FT-IR of pure MCM-41 (Fig. 6)

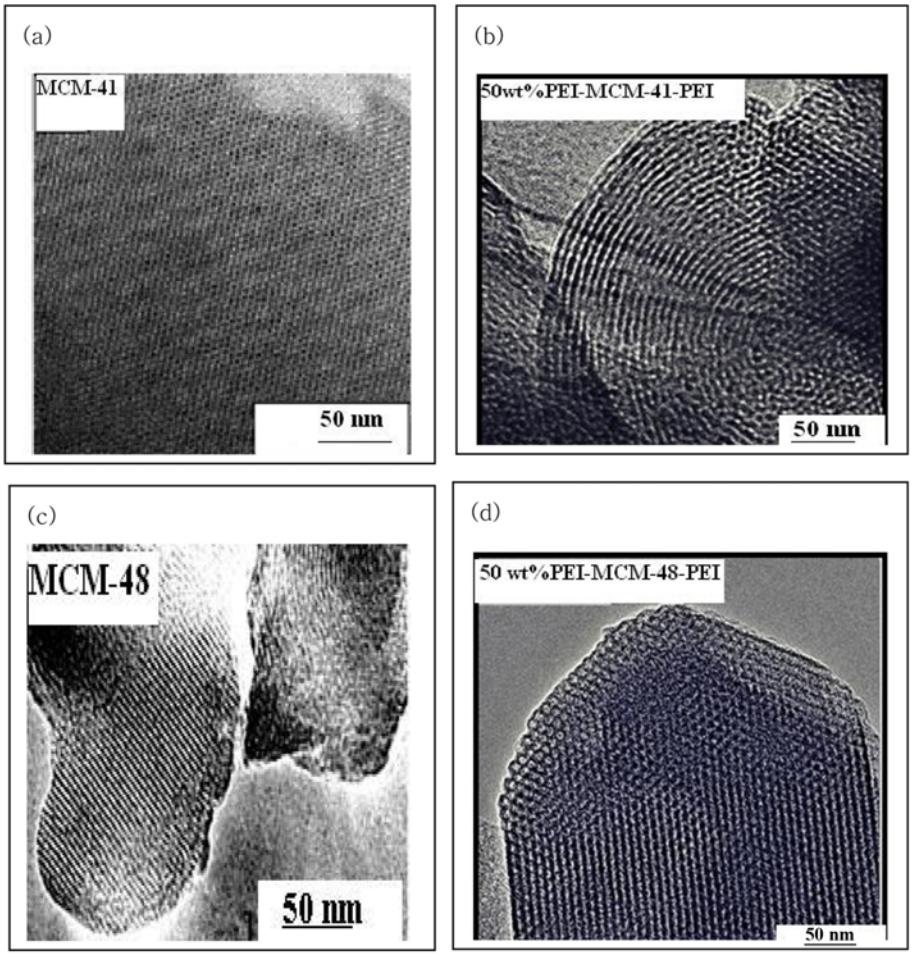

Fig. 8. TEM image of materials: (a) MCM-41, (b) 50 wt% PEI-MCM-41-PEI. (c) MCM-48, (d) 50 wt% PEI-MCM-48-PEI.

shows broad band around 3,700 cm^{-1}, due to -OH stretching of water and for the weak single Si-OH groups derived from the germinal Si-OH groups. The peak of bending mode of water is observed at 1,625 cm^{-1}. The unresolved peaks at higher energy position are due to defective Si-OH group. The samples also exhibit a weak band around 800 cm^{-1} attributed to the Si-O-Si stretching vibration and 950 cm^{-1}, which is assigned to the symmetric stretching vibration of the Si-OH groups. The spectrum of 50 wt% PEI-MCM-41-PEI (Fig. 6) shows all the characteristics bands of MCM-41. In addition, the weak band at 1,500 cm^{-1} is attributed to asymmetric and symmetric bending of the 1° amines, whereas the weak band around 1,600 cm^{-1} is assigned to the bending mode of 2° amines. The presence of two weak bands between 2,800-2,950 cm^{-1} is at- tributed to C-H stretching [38]. The presence of these characteristic bands of 1° and 2° amines confirms that PEI is impregnated on the surface of MCM-41 and MCM-48. For the FT-IR spectra of MCM-48 (Fig. 7), similar characteristic bands appear which are present in MCM-41. The spectra of 50 wt% PEI-MCM-48-PEI (Fig. 7) also possess the bands which are present in 50 wt% PEI-MCM-41-PEI samples. But the most important difference observed is that the intensity of absorption bands assigned to 1° and 2° amines is higher in PEI loaded MCM-48 materials than PEI loaded on MCM-41 materials. Therefore, PEI impregnated on MCM-48 sample is expected to have increased CO_2 adsorption capacity than MCM-41 samples since CO_2 adsorption capacity is directly proportional to active 1° and 2° amines. The FT-IR studies also support XRD and N_2 adsorption-desorption results, which claim that MCM-48 is a superior material as compared to MCM-41 for loading of PEI.

The TEM pictures of MCM-41 and MCM-48 are presented in Fig. 8(a)-(d). The TEM photograph of MCM-41 (Fig. 8(a)) shows that the size and morphology of the mesoporous catalysts with highly ordered honeycomb-like regular arrangement of hexagonal pores on the molecular sieves. The pictures also show the orderly growth of pure hexagonal phase with well-defined sites and one-dimensional mesoporous parallel channels within the MCM-41. The TEM result confirms that the MCM-41 are pure phases with short and ordered mesoporous channels. TEM imaging of 50 wt% PEI-MCM-41-PEI (Fig. 8(b)) shows similarity with TEM image of MCM-41,

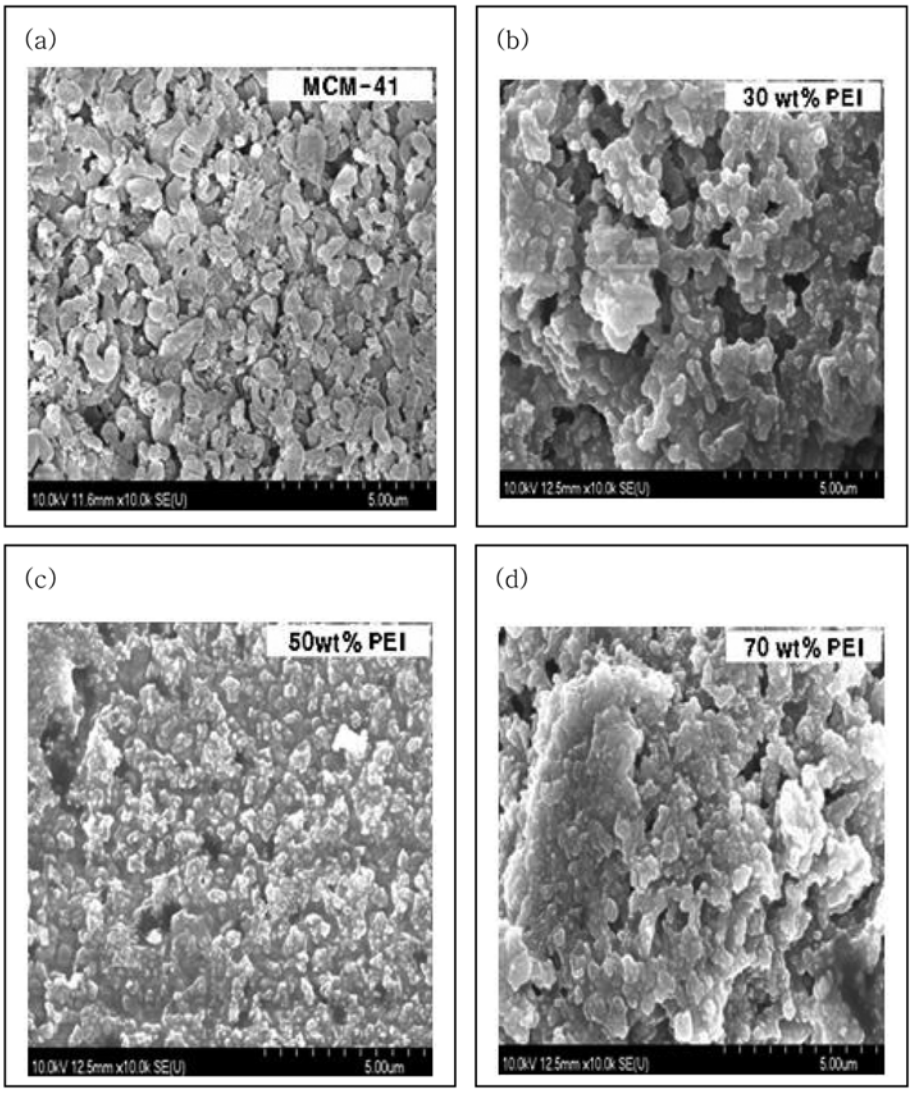

Fig. 9. SEM image of materials; (a) MCM-41, (b) 30 wt% PEI-MCM-41-PEI. (c) 50 wt% PEI-MCM-41-PEI, (d) 70 wt% PEI-MCM-41-PEI.

which indicates that after loading of 50 wt%PEI, the well ordered and honeycomb-like regular arrangement of hexagonal pores structure is maintained. The TEM image of MCM-48 (Fig. 8(c)) reveals that parts of mesoporous particles are well aligned with respect to the electron beam and show the periodicity of the MCM-48 silica framework. The pictures also show the orderly growth of pure cubic phase with well-defined sites and one-dimensional mesoporous parallel channels within the MCM-48. TEM imaging of 50 wt% PEI-MCM-48-PEI (Fig. 8(d)) shows similarity with TEM image of MCM-48 with little irregularity, which indicates that after loading of 50 wt% PEI, the well ordered and regularly arranged cubic phase of MCM-48 structure is changed slightly. Both PEI impregnated materials still retained a well ordered porous nature and no appreciable amount of aggregation is observed in TEM imaging. But, a very small disorder and worm-like channel structures are observed in PEI impregnated materials. Apparently, disordered regions could indeed be disordered, but might also result from an unfavorable axis chosen for the image.

The surface morphology of the materials is studied by SEM. The SEM image of MCM-41 is reported in Fig. 9(a). The particles are flat and hexagonal-to-round, resulting in a disc-like morphology. It is evident from the micrograph that the particles have a uniform size. The SEM of 30 wt% PEI-MCM-41-PEI (Fig. 9(b)) shows a large crystal from the scattered crystals with bright shiny spots. These shiny spots likely result from charging because silica is not a conductor. From this image one can see that primary particles agglomerate to form larger, micron-size particles. The SEM of 50 wt% PEI-MCM-41-PEI (Fig. 9(c)) shows PEI is uniformly distributed on the surface. For this case, the primary particles are fused together, although this material had smaller aggregates compared to the other two materials of 30 wt% and 70 wt% PEI loading. The SEM of 70 wt% PEI-MCM-41-PEI (Fig. 9(d)) shows a similar morphology to 30 wt% PEI-MCM-41-PEI but with a thick PEI layer and large aggregates. Unlike the case of 50 wt% PEI-MCM-41-PEI dispersion, the PEI was not uniformly distributed in 70 wt% PEI-MCM-41-PEI material. The SEM image of MCM-48 is reported in Fig. 10(a). The particles show an irregular crystallization of small and large Si crystals. The SEM of 30 wt% PEI-MCM-48-PEI (Fig. 10(b)) shows

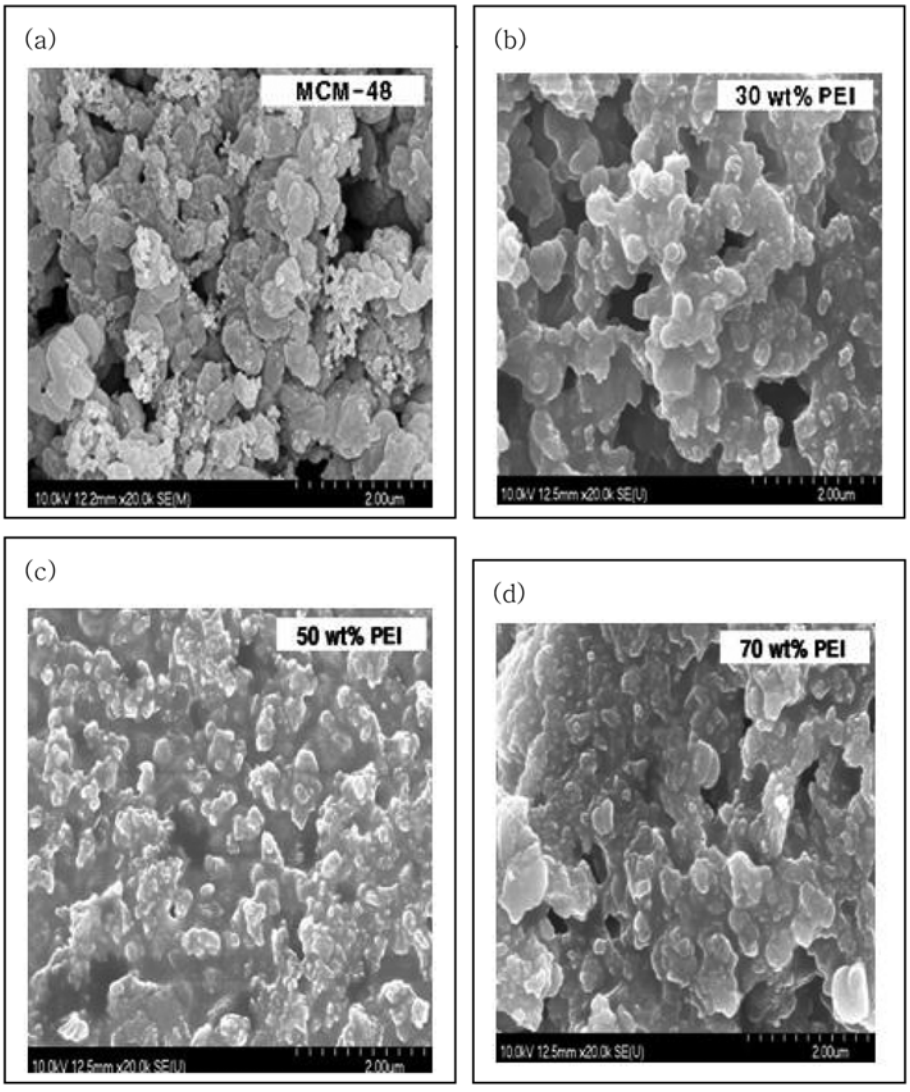

Fig. 10. SEM image of materials; (a) MCM-48, (b) 30 wt% PEI-MCM-48-PEI, (c) 50 wt% PEI-MCM-48-PEI, (d) 70 wt% PEI-MCM-48-PEI.

a large crystal from the scattered crystals with bright shiny spots, which indicates that the PEI is distributed on the surface and surface morphology is completely changed. From this image one can see that primary particles agglomerate to form larger, micron-size particles. The intensity of agglomeration is very high in this material. The SEM of 50 wt% PEI-MCM-48-PEI (Fig. 10(c)) shows PEI is uniformly distributed on the surface. For this case, the primary particles are fused together, although this material had smaller aggregates compared to the other two materials of 30 wt% and 70 wt% PEI loading. The SEM of 70 wt% PEI-MCM-48-PEI (Fig. 10(d)) shows a similar morphology to 30 wt% PEI-MCM-48-PEI but with a thick PEI layer and large sized aggregates. Unlike the case of 50 wt% PEI-MCM-48-PEI dispersion, the PEI was not uniformly distributed in 70 wt% PEI-MCM-48-PEI material.

Figs. 11(a)-(d) and 12(a)-(d) show the results of the adsorption test conducted to separate CO_2 using the PEI-impregnated mesoporous materials. W_0 represents the weight of the sample and W represents the weight of the sample after adsorbing CO_2. Figs. 11(a)-(d) show the CO_2 adsorption of the PEI-impregnated MCM-41 adsorbent at 40, 60, 80 and 100 °C, respectively. They showed quick adsorption until 10 minutes before, and then low increasing width thereafter. The CO_2 adsorption increased as wt% loading of PEI increased, and as temperature increased and then decreased after 80 °C. At 80 °C, the adsorption was 47.5, 69.4 and 84 mg/g-adsorbent, for 30 wt% PEI-MCM-41-PEI, 50 wt% PEI-MCM-41-PEI and 70 wt% PEI-MCM-41-PEI, respectively. Figs. 12(a)-(d) show CO_2 adsorption at at 40, 60, 80 and 100 °C after impregnating PEI in MCM-48 at different wt% of PEI. They show levels of adsorption similar to MCM-41. At 80 °C, the adsorption was 69.4, 110.1 and 86.7 mg/g for 30 wt% PEI-MCM-48-PEI, 50 wt% PEI-MCM-48-PEI and 70 wt% PEI-MCM-48-PEI, respectively. For each material, CO_2 adsorption increased as wt% of PEI increased. Different materials had different rates of adsorption. The maximum adsorption was shown at 70 wt% immersion of PEI. And MCM-48 showed more adsorption than MCM-41. The results coincide with the MEA test results, which show the shape and size of the pores formed during the synthesis of the material and the type of immersed material that affects CO_2 adsorption.

Fig. 13 shows the comparison of CO_2 adsorption at 60 and 80 °C with different wt% loading of PEI impregnation on MEA and MCM-48. The results show a significant difference in adsorption between MEA and PEI impregnation. This is because CO_2 adsorption increases as the sites to bond with CO_2 increase, as PEI consists of numerous side branches with huge N-H molecules. Therefore, more CO_2 can be adsorbed even at a high temperature compared to MEA. While MEA adsorbs 1 mol of CO_2 for every 2 mol of nitrogen mole-

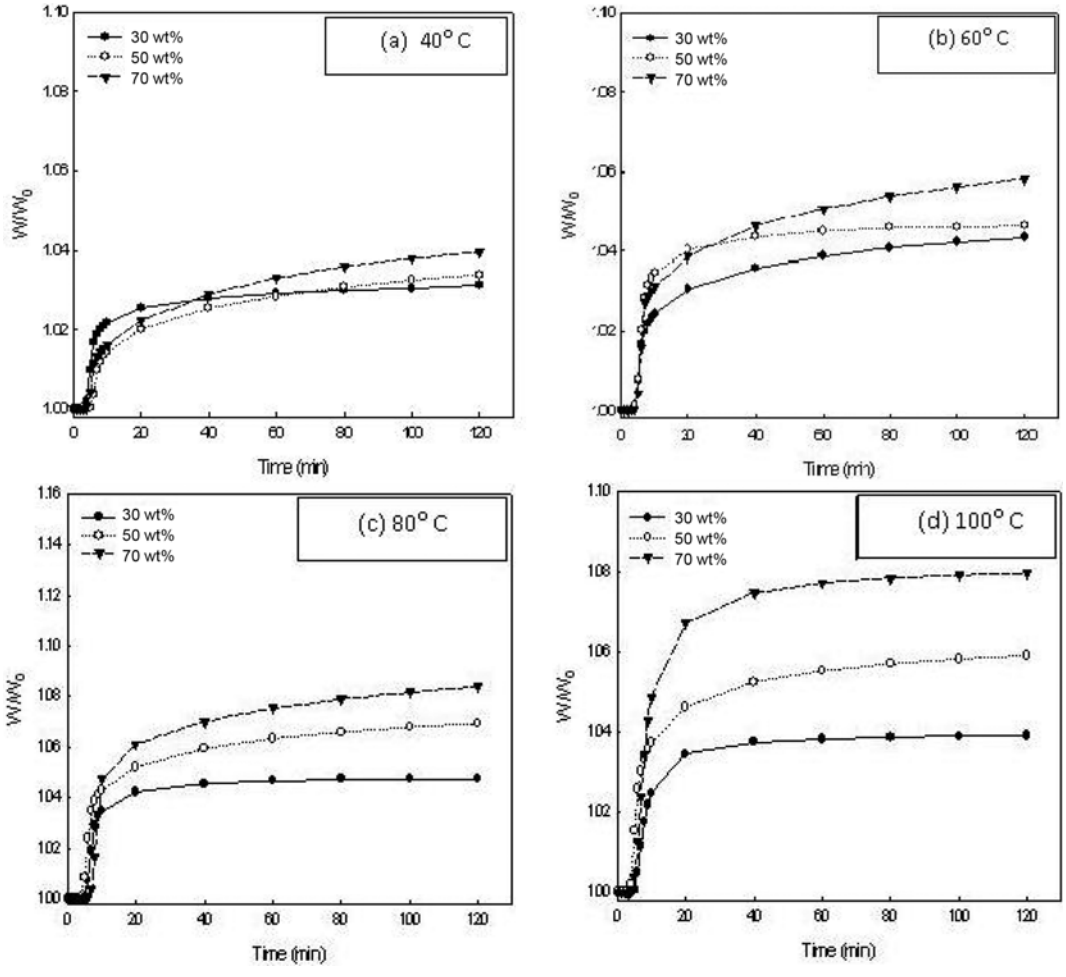

Fig. 11. CO_2 adsorption curves of PEI impregnated MCM-41 at different temperature.

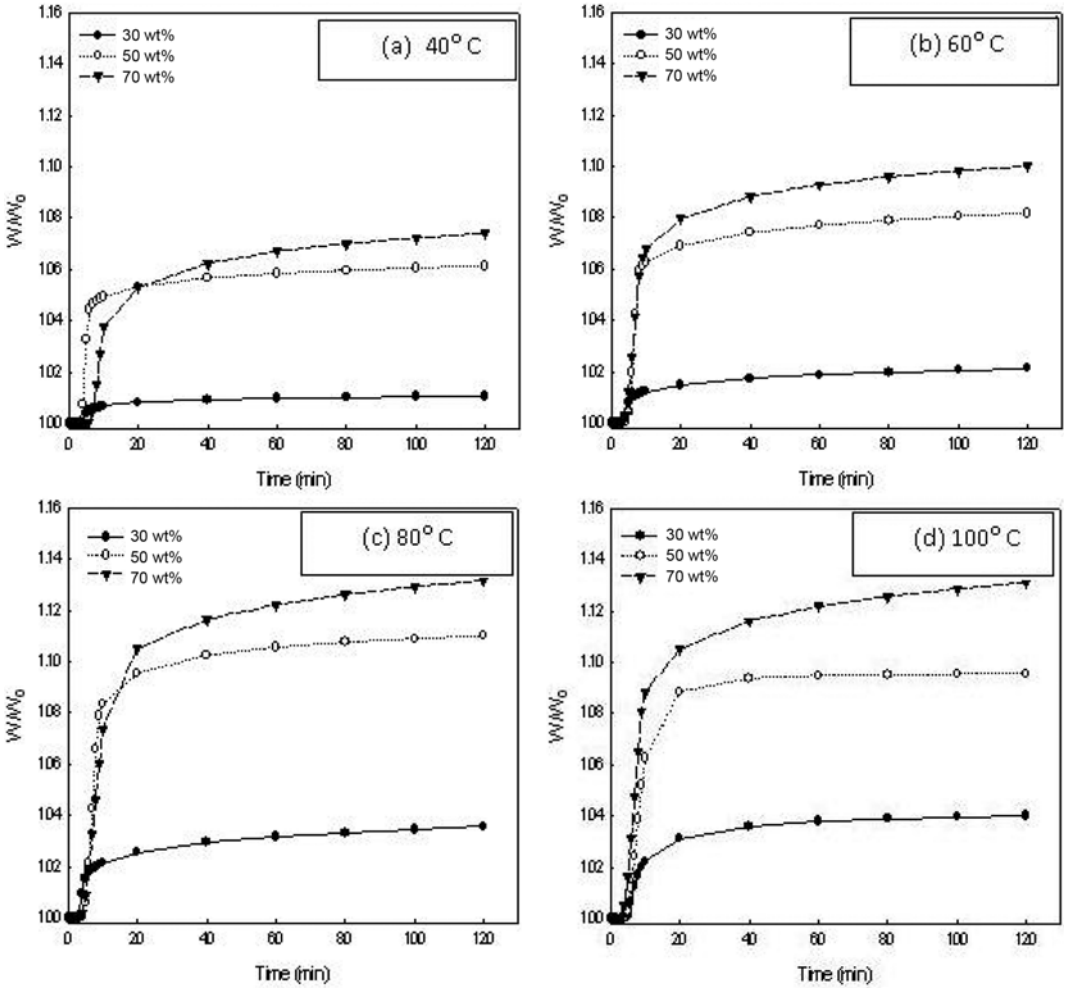

Fig. 12. CO_2 adsorption curves of PEI impregnated MCM-48 at different temperature.

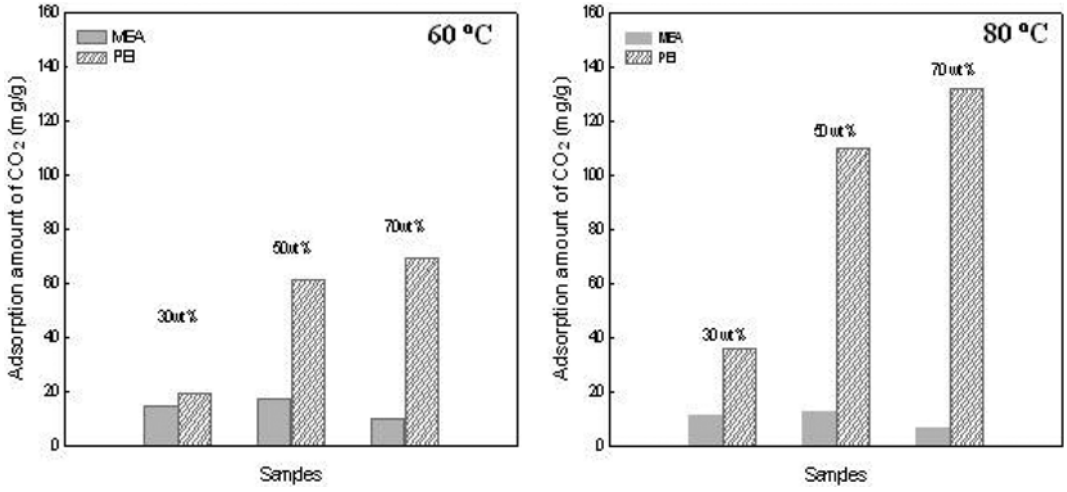

Fig. 13. Comparison of CO_2 adsorption capacity of MEA and PEI with different wt% loading at different temperature.

cule, PEI adsorbs 1 mol of CO_2 for each mol of nitrogen molecule. Thus adsorption of CO_2 increases by 1 mol when a polymer PEI is used.

Figs. 14(a)-(b) show the synergy effect of the mesoporous material and amine in adsorbing CO_2, using Eqs. (1) and (2) as presented by Xu [36]. Figs. 14(a) and 14(b) show the linear adsorption and calculated synergetic adsorption of MCM-41 and MCM-48, respectively. The linear adsorption is calculated by CO_2 adsorption

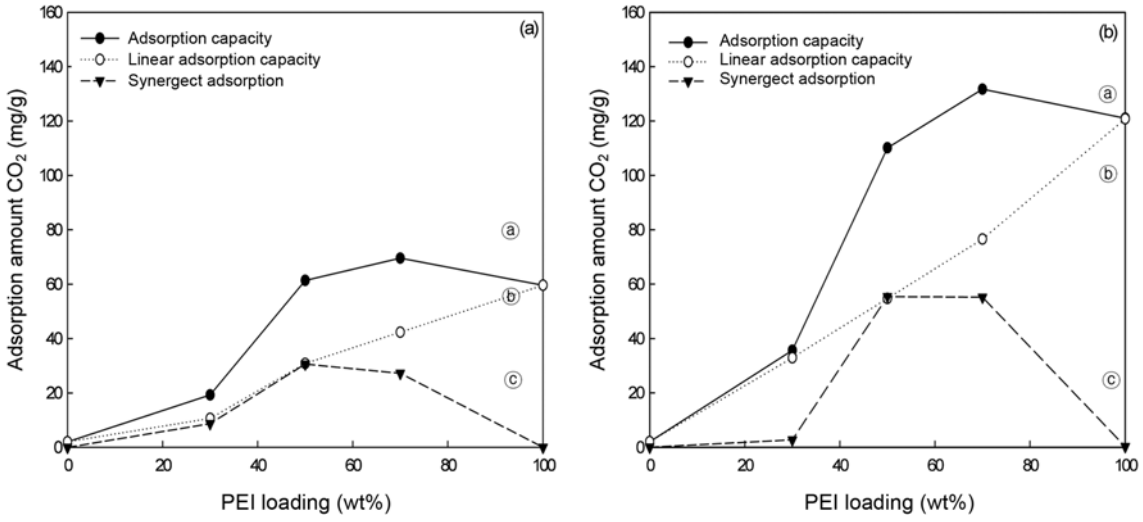

Fig. 14. Synergetic effect of mesoporous materials on the adsorption of CO_2 MEA and PEI impregnated: (a) MCM-41, (b) MCM-48.

of each material before impregnation. As the wt% of PEI increases, CO_2 adsorption increases, showing a linear graph. The synergetic adsorption gain is calculated by the difference in CO_2 adsorption according to the linear adsorption and concentration. Compared to linear adsorption, the highest synergetic adsorption gain could be attained at 50 wt% of PEI impregnation. Calculation of amine efficiency to mesoporous material according to immersion concentration in Eq. (3) showed the efficiencies of 0.6, 1.2 and 0.9 for MCM-41 and 1.2, 2.2 and 1.9 for MCM-48, as shown in Table 2. The calculation of amine efficiency shows that the optimum impregnation condition was 50 wt% PEI. The SEM results shown in Figs. 9 and 10 also indicate that the number of PEI particles on the surface of the mesoporous material increases as the extent of wt% of PEI increases, but PEI was uniformly distributed on the surface of mesoporous material in the case of 50 wt% PEI loading, indicating that the amount that can be accepted by the adsorbent is limited even when a high amount of amine is available.

3. Effect of PEI Loadings

Before the PEI was loaded, MCM-41 and MCM-48 supports alone showed a CO_2 adsorption capacity of 8.6 and 8.9 mg/g-adsorbent, respectively. The low adsorption capacity was caused by the weak interaction between CO_2 and Si-MCM-41/48 at relative high temperature. To strengthen the interaction between CO_2 and Si-MCM-41/48, branched polymeric substances with numerous CO_2-capturing sites, were loaded into the Si-MCM-41/48 channels. The influence of PEI loading on the CO_2 adsorption performance of wt%-PEI-MCM-41-PEI and wt%-PEI-MCM-48-PEI was investigated in pure CO_2 atmosphere at 40, 60, 80 and 100 °C and results are reported in Figs. 11 and 12. Surprisingly, the PEI had no significant contribution on CO_2 adsorption capacity at low PEI loading. When the PEI loading was 30 wt%, the CO_2 adsorption capacity was only 20 and 38 mg/g-adsorbent at 80 and 100 °C. At 50 wt% PEI loading, the adsorption capacity was 62 and 114 mg/g-adsorbent at 80 and 100 °C. Whereas, the adsorption capacity of pure PEI at 50 wt% loading was also 111 mg/g-adsorbent. The mesoporous materials of Si-MCM-41/48 showed a synergic effect on the adsorption of CO_2 by PEI. The highest adsorption capacity of 70 and 132 mg/g-adsorbent was obtained at 80 and 100 °C with 70 wt% loading of PEI.

The desorption was complete for all the wt% PEI-MCM-41/48-PEI adsorbents as well as the MCM-41/48 supports. However, the adsorption for pure PEI was slow and was not complete compared to the desorption time of the wt% PEI-MCM-41/48-PEI adsorbents. The fast desorption of CO_2 from the wt% PEI-MCM-41/48-PEI materials can be explained by the uniform and high dispersion of the PEI in MCM-41/48 channels as shown by powder XRD, N_2 adsorption-desorption, TGA, TEM, SEM characterization results.

The above-mentioned various characterization techniques and CO_2 adsorption capacity results showed that MCM-48 is a better support compared to MCM-41 for the loading of PEI. Therefore, further studies have been performed with PEI loaded on MCM-48 materials only.

DISCUSSION

To reveal any synergetic effects between MCM-41/48 and PEI on CO_2 adsorption, the linear adsorption capacity and the synergetic adsorption gain were calculated by Eqs. (1), (2), and (3), respectively, given below, reported by Song et al. [36].

Linear adsorption capacity (mg adsorbate/g-adsorbent)
=[(MCM-41/48 weight percentage in the adsorbent
×adsorption capacity of pure MCM-48)
+(PEI weight percentage in the adsorbent
×adsorption capacity of pure PEI)] (1)

Synergetic adsorption gain (mg adsorbate/g-adsorbent)
=adsorption capacity of the adsorbent
−lineat adsorption capacity (2)

Amine efficiency=CO_2 adsorption/content of amine (3)

The linear adsorption capacity and the synergetic adsorption gain of MEA and PEI loaded MCM-48 were calculated and compared in Fig. 14. This indicates that up to 20 wt% loading of MEA and PEI on MCM-48, the synergetic adsorption gain was much less,

close to 15 mg/g-adsorbent, and CO_2 adsorption capacity was almost same. When MEA and PEI loading was higher than 30 wt%, a synergetic adsorption gain was observed, which indicated that MEA and PEI modified MCM-48 began to act as a CO_2 molecular basket [36]. The highest synergetic gain was obtained at the MEA and PEI loading of 50 wt%, while the synergetic adsorption gain decreased at the PEI loading of 75 wt%. The synergetic gain was significantly high in PEI samples compared to MEA. This further proved that, for loading purpose, PEI is a better and more intelligent choice compared to other amines.

The adsorption capacity of the PEI only in the "molecular basket" adsorbent was calculated by Eq. (4), which was earlier reported by Song et al. [36]. This can be represented as follows:

PEI adsorption capacity (mg adsorbate/g-PEI)
=[adsorption capacity of the adsorbent
−(MCM-48 weight percentage in the adsorbent
×adsorption capacity of pure MCM-48)]
/(PEI weight percentage in the adsorbent) (4)

The calculated PEI adsorption capacity is 248 mg/g-PEI for 50 wt% PEI-MCM-48-PEI and 171 mg/g-PEI for 70 wt% PEI-MCM-48-PEI. Since the 70 wt% PEI-MCM-48-PEI was prepared by 25 wt% of MCM-41 and 75 wt% of PEI, we can assume that 25 wt% of the PEI is loaded into the pores of the MCM-48 and the other 50 wt% of the PEI is coated on the external surface of the MCM-48. If we assume that the PEI loaded into the MCM-48 channel shows the same adsorption capacity as that of the 50 wt% PEI-MCM-48-PEI, the adsorption capacity of the PEI that was coated on the external surface of MCM-48 for 70 wt% PEI-MCM-48-PEI can be calculated and is found to be only 150 mg/g-PEI. The adsorption capacity for the PEI coated on the external surface of the MCM-48 was much lower than that of the 50 wt% PEI-MCM-48-PEI (248 mg/g-PEI) when the PEI fully filled in the channels of the MCM-48, which confirmed that only when the PEI was loaded into the channels of the mesoporous molecular sieve did the MCM-48 show the highest synergetic effect and proved that the "molecular basket" concept resulted in the significant improvement on the CO_2 adsorption by PEI. The adsorption capacity for the PEI coated on the external surface of the crystal was slightly greater than that of the pure PEI of 110 mg/g-PEI. When the PEI is coated on the crystal surface, more adsorption sites will be exposed to the adsorbate. Therefore, the adsorption capacity will be higher than that of the bulk PEI. This can also be verified by the CO_2 adsorption capacity of PEI coated on other high-surface-area materials such as silica gel. When the PEI was coated on a high-surface-area silica gel (500 m^2/g) and the PEI loading was 50%, the CO_2 adsorption capacity was only 152 mg/g-PEI, slightly higher than that of the bulk PEI and much lower than that of the "molecular basket" adsorbent with the same PEI loading, which also verified that only when the PEI was loaded into the channels of the mesoporous molecular sieve did the MCM-48 show the highest synergetic effect on the adsorption of CO_2. The CO_2 adsorption capacity of Silica Gel-PEI was nearly identical to that of the calculated CO_2 adsorption capacity on the external surface of the MCM-48. Song et al. [36] and Satyapal et al. [37] also observed the same phenomenon when they loaded the PEI on MCM-41 and the high-surface-area solid polymethyl methacrylate polymeric support, respectively.

Compared with conventional adsorbents, the "molecular basket" showed better CO_2 adsorption performance at relatively high temperature. Table 3 lists the CO_2 adsorption performance of zeolite, activated carbon, PEI/polymer composite and "molecular basket" adsorbent. The amine modified "molecular basket" adsorbents shows

Table 3. Comparison of CO_2 adsorption performance of molecular basket adsorbent and other adsorbents

Adsorbents	Temp. (°C)	Pressure (atm)	Adsorption capacity (mg CO_2/g adsorbent)	CO_2/N_2 or CO_2/CH_4 selectivity	Ref.
Si-MCM-41	25	1	27.3	-	36
Si-MCM-41	75	1	8.6	-	36
Si-MCM-41	75	0.149	6.3	2.9 (CO_2/N_2)	35
Al-MCM-41-100	75	1	7.6	-	36
Al-MCM-41-500	75	1	7.5	-	36
Si-MCM-41-PEI-50	25	1	32.9	-	36
Si-MCM-41-PEI-50	75	1	112	-	36
50 wt%PEI-MCM-48-PEI	80	1	114	-	This study
Si-MCM-41-PEI-50	75	0.149	89.2	>1,000 (CO_2/N_2)	35
Al-MCM-41-100-PEI-50	75	1	127	-	36
Al-MCM-41-500-PEI-50	75	1	121	-	36
Zeolite 13 X	25	1	168	-	39
Zeolite 4 A	25	1	135	-	39
Activated carbon	25	1	110	-	39
Norit RBI activated carbon	21.5	1	108	~2 (CO_2/CH_4)	41
Norit RBI activated carbon	75	1	40	~2 (CO_2/CH_4)	41
Activated carbon	20	1	88	~2 (CO_2/CH_4)	40
Norit RBI activated carbon	25	1	140.8	~1.9 (CO_2/CH_4)	42
PEI-silica gel	75	1	78.1	-	36
PEI-polymer	~50	0.02	~40	-	43

superior CO_2 adsorption capacity as compared to pure mesoporous materials.

CONCLUSIONS

A novel CO_2 "molecular basket" adsorbent based on polyethylenimine (PEI)-modified mesoporous MCM-48 type (MCM-48-PEI) has been synthesized that shows the highest CO_2 adsorption capacity of 248 mg/g-PEI, which is about 30 times higher than that of the MCM-48 and is about 2.3 times that of the pure PEI.

When the PEI loading was higher than 30 wt%, the mesoporous MCM-48 showed a synergetic effect on the adsorption of CO_2 by PEI. The maximum synergetic effect was obtained when the PEI loading was 50 wt%. When the PEI loading was 75 wt%, the PEI was coated on the external surface of MCM-48 and the synergetic effect decreased. The experiment results showed that, although the dispersion of PEI on the high surface area materials could increase the adsorption capacity, it was the synergetic effect between PEI and MCM-48 pore channels, in the case of CO_2 "molecular basket", which contributes to a major increase in the CO_2 adsorption capacity.

The CO_2 adsorption at 40, 60, 80 and 100 °C showed that adsorption increased as the temperature increased up to 100 °C, after which adsorption decreased. Different rates of CO_2 adsorption were also observed in different synthesized materials. MCM-48 showed more adsorption than MCM-41, and PEI loaded on MCM-48 showed the highest adsorption with 114 mg-CO_2/gr-sorbent. This is probably due to the difference in pores created during the synthesis.

The significant difference in CO_2 adsorption between MEA and PEI loading may be attributed to the fact that PEI consists of numerous side branches composed of huge N-H molecules, thus increasing the number of sites to bond CO_2. Therefore, it can adsorb more CO_2 than MEA even at a high temperature. Where MEA can adsorb 1 mol of CO_2 for every 2 mol of N molecule, PEI can adsorb 1 mol of CO_2 for every 1 mol of N molecule. As such, a PEI adsorbent with more N-H side branches can adsorb more CO_2.

ACKNOWLEDGEMENTS

This research was supported by a grant (code CE3-101) from the Carbon Dioxide Reduction & Sequestration Research Center, one of the 21st-Century Frontier Programs funded by the Ministry of Science and Technology of the Korean government.

REFERENCES

1. C. Song, *Catal. Today*, **115**, 2 (2006).
2. Climate Change 2001: *The scientific basis, Contribution of working group I to the third assessment report of the intergovernmental panel on climate change*, Cambridge, United Kingdom and New York (NY, USA): Cambridge University Press (2001).
3. P. Forster, V. Ramaswamy, P. Artaxo, T. Berntsen, R. Betts, D. W. Fahey and J. Haywood, Climate change 2007: *The physical science basis*, Intergovernmental Panel on Climate Change. Cambridge: Cambridge University Press (2007).
4. D. Shekhawat, D. R. Luebke and H. W. Pennline, *A topical report: A review of carbon dioxide selective membranes*, National Energy Technology Laboratory, United States Department of Energy (2003).
5. M. P. Bernal, J. Coronas, M. Menendez and J. Santamaria, *AIChE J.*, **50**, 127 (2004).
6. H. Lin and B. D. Freeman, *J. Mol. Struct.*, **739**, 57 (2005).
7. Y. Sakamoto, K. Nagata, K. Yogo and K. Yamada, *Micropor. Mesopor. Mater.*, **101**, 303 (2007).
8. P. Kumar, S. Kim, J. Ida and V. V. Guliants, *Ind. Eng. Chem. Res.*, **47**, 201 (2008).
9. M. T. Ho, G. A. Allinson and D. E. Wiley, *Ind. Eng. Chem. Res.*, **47**, 1562 (2008).
10. S.-W. Park, D.-S. Suh, K.-S. Hwang and H. Kumazawa, *Korean J. Chem. Eng.*, **4**, 285 (1997).
11. F. Zheng, D. N. Tran, B. J. Busche, G. E. Fryxell, R. S. Addleman, T. S. Zemanian and C. L. Aardahl, *Ind. Eng. Chem. Res.*, **44**, 3099 (2005).
12. M. L. Gray, Y. Soong, K. J. Champagne, H. Pennline, J. P. Baltrus, R. W. Stevens Jr., R. Khatri, S. S. C. Chuang and T. Filburn, *Fuel. Proc. Technol.*, **86**, 1449 (2005).
13. R. Bounaceur, N. Lape, D. Roizard, C. Vallieres and E. Favre, *Energy*, **31**, 2556 (2006).
14. R. S. Franchi, P. J. E. Harlick and A. Sayari, *Ind. Eng. Chem. Res.*, **44**, 8007 (2005).
15. G. P. Knowles, J. V. Graham, S. W. Delaney and A. L. Chaffee, *Fuel. Proc. Technol.*, **86**, 1435 (2005).
16. S. Kim, J. Ida, V. V. Guliants and Y. S. Lin, *J. Phys. Chem. B*, **109**, 6287 (2005).
17. V. V. Guliants, M. A. Carreon and Y. S. Lin, *J. Membr. Sci.*, **235**, 53 (2004).
18. C. Knofel, J. Descarpentries, A. Benzaouia, V. Zelenak, S. Mornet, P. L. Llewellyn and V. Hornebecq, *Micropor. Mesopor. Mater.*, **99**, 79 (2007).
19. N. Hiyoshi, K. Yogo and T. Yashima, *Stud. Surf. Sci. Catal.*, **153**, 417 (2004).
20. G. P. Knowles, S. W. Delaney and A. L. Chaffee, *Stud. Surf. Sci. Catal.*, **156**, 887 (2005).
21. J. S. Beck, J. C. Vartuli, W. J. Roth, M. E. Leonowicz, C. T. Kresge, K. D. Schmitt, C. T.-W. Chu, D. H. Olson, E. W. Sheppard, S. B. McCullen, J. B. Higgins and J. L. Schlenker, *J. Am. Chem. Soc.*, **114**, 10834 (1992).
22. K. Schumacher, P. I. Ravikovitch, A. D. Chesne, A. V. Neimark and K. K. Unger, *Langmuir*, **16**, 4648 (2000).
23. M. Hartmann and C. Bischof, *J. Phys. Chem. B*, **103**, 6230 (1999).
24. X. S. Zhao, G. Q. Lu and X. Hu, *Colloids Surf. A*, **179**, 261 (2001).
25. S. Kawi and M. Te, *Catal. Today*, **44**, 101 (1998).
26. K. Schumacher, M. Grun and K. K. Unger, *Micropor. Mesopor. Mater.*, **27**, 201 (1999).
27. A. Sayari, *J. Am. Chem. Soc.*, **122**, 6504 (2000).
28. T. Tatsumi, K. A. Koyano, Y. Tanaka and S. Nakata, *J. Porous Mater.*, **6**, 13 (1999).
29. H. Yoshitake, T. Yokoi and T. Tatsumi, *Chem. Mater.*, **14**, 4603 (2002).
30. G. E. Fryxell, J. Liu, T. A. Hauser, Z. Nie, K. F. Ferris, S. Mattigod, M. Gong and R. T. Hallen, *Chem. Mater.*, **11**, 2148 (1999).
31. X. Lin, G. K. Chuah and S. J. Jaenicke, *J. Mol. Catal. A: Chem.*, **150**, 287 (1999).
32. S. C. Shen, X. Chen and S. Kawi, *Langmuir*, **20**, 9130 (2004).
33. H. Y. Huang, R. T. Yang, D. Chinn and C. L. Munson, *Ind. Eng.*

Chem. Res., **42**, 2427 (2003).
34. A. L. Chaffee, S. W. Delaney and G. P. Knowles, *Abstr. Pap. Am. Chem. Soc.*, 223 (2002).
35. X. Xu, C. Song, J. M. Anderson, G. B. Miller and A. W. Scaroni, *Energy Fuels*, **16**, 1463 (2002).
36. X. Xu, C. Song, J. M. Andresen, B. G. Miller and A. W. Scaroni, *Micropor. Mesopor. Mater.*, **62**, 29 (2003).
37. X. Xu, C. Song, B. G. Miller and A. W. Scaroni, *Fuel. Proc. Technol.*, **86**, 1457 (2005).
38. Xiaoxing Wang, V. Schwartz, J. C. Clark, X. Ma, S. H. Overbury, X. Xu and C. Song, *J. Phys. Chem. C*, **113**, 7260 (2009).
39. R. V. Siriwardane, M. S. Shen, E. P. Fisher and J. A. Poston, *Energy Fuels*, **15**, 279 (2001).
40. K. Berlier and M. Frere, *J. Chem. Eng. Data*, **42**, 533 (1997).
41. R. van der Vaart, C. Huiskes, H. Bosch and T. Reith, *Adsorption*, **6**, 311 (2000).
42. F. Dreisbach, R. Staudt and J. U. Keller, *Adsorption*, **5**, 215 (1999).
43. S. Satyapal, T. Filburn, J. Trela and J. Strange, *Energy Fuels*, **15**, 250 (2001).